Marine Structures 44 (2015) 211–231

Contents lists available at ScienceDirect

Marine Structures

journal homepage: www.elsevier.com/locate/marstruc

Dynamic analysis of risers using a novel multilayered pipe beam element model

L.L. Aguiar [a, *], C.A. Almeida [b], G.H. Paulino [c]

[a] Petrobras, CENPES – Research and Development Center, Rio de Janeiro, Brazil
[b] Department of Mechanical Engineering, Pontifical Catholic University of Rio de Janeiro, Rio de Janeiro, Brazil
[c] Department of Civil and Environmental Engineering, University of Illinois, Urbana, IL 61801, USA

ARTICLE INFO

Article history:
Received 20 December 2014
Received in revised form 26 August 2015
Accepted 28 August 2015
Available online 26 October 2015

Keywords:
Multi-layered pipe beams
Riser analysis
Finite element
Nonlinear dynamic analysis

ABSTRACT

In this paper a recently proposed formulation for the multilayered pipe beam element is extended to dynamic analysis of risers. Derivations of hydrostatic and hydrodynamic loadings due to internal and external fluid acting on each element layer are presented. Mass and damping matrices, associated to each element layer, are properly derived by adding their respective contributions to the expression of the virtual work due to external loading. The finite element implementation allows for the numerical representation of either bonded or unbonded multilayered risers, including small slip effects between layers. A number of numerical examples have been carried out and the results show the accuracy and efficiency of the new element formulation, even in large scale riser analysis. Moreover, we establish a few benchmarks using multilayered pipes and risers.

1. Introduction

Several types of risers are currently in use in the petroleum industry, including steel catenary risers (SCR) in deep water production systems, top-tensioned risers in dry completion systems, riser towers where multiple pipes are used in a single assembly and flexible riser configurations that can be used both in shallow and deep waters. For standard homogeneous cross sections, considering the length to diameter ratio, the riser kinematics of deformation is adequately represented by classical Euler-Bernoulli beam model [12,23]. However, in most of the cases, such as in lined and cladded pipes, thermal insulation coatings, pipe-in-pipe or any kind of pipe made of composite materials, the riser

* Corresponding author.
E-mail address: ludiaguiar@gmail.com (L.L. Aguiar).

http://dx.doi.org/10.1016/j.marstruc.2015.08.004
0951-8339/

cross section is formed by layers of different materials, which should be properly and discretely represented in the pipe analysis model. In recent years, formulations for the representation of multilayered beams have been proposed by many authors [5,6,9–11,15,24,25,31], in most cases restricted to the analysis of rectangular laminated beams, subjected to static loadings. In some articles, as those by Xu et al. [28] and Wu et al. [27], the formulation also considers the dynamics of the beam element, but still restricted to small displacement analyses. In this work the multilayered pipe beam formulation recently proposed by Aguiar et al. [2], for the static analysis of risers, has been extended to include dynamic effects. The element considers the nonlinear behavior of multilayered pipes in general 3-D large displacement analysis by using an updated Lagrangian formulation that includes large displacements and rotations [2]. Constant transverse shear strains, along the element length, are also considered by adding two generalized degrees-of-freedom to the conventional axial, bending and torsional ones, which are statically condensed throughout the solution procedure. Interface binding condition effects that include slip with friction between layers are accounted in the formulation by defining a proper constitutive relation for the interface material. In the next section, a short review of the element formulation is presented, following the derivations in Ref. [2], but including inertia and damping effects. In the third section, derivations for static loading such as internal fluid weight, pipe weight and buoyancy forces, as well as hydrodynamic loadings, due to external fluid flow, are derived. Section four presents the details of the element numerical implementation for 3D analysis. A few test analyses allowing the evaluation of the multilayered pipe element performance in dynamics are presented in section five. Finally, some concluding remarks are given in section 6.

2. Finite element formulation

A numerical formulation for the multilayered pipe element is set by adding each layer strain energy contributions - associated to linear and nonlinear strain measures - to the appropriate straining at the each interface material between layers. Considering a single layer, the equilibrium condition at time $(t+\Delta t)$, using the Principle of Virtual Work (PVW) for an updated Lagrangian formulation, gives [4]:

$$\int_V S_{ij}^{t+\Delta t}\ \delta\ \varepsilon_{ij}^{t+\Delta t} dV = \Re^{t+\Delta t} \tag{1}$$

where $S_{ij}^{t+\Delta t}$ is the second Piola–Kirchoff stress tensor [18]; $\varepsilon_{ij}^{t+\Delta t}$ is the Green–Lagrange strain tensor [18]; and $\Re^{t+\Delta t}$ is the virtual work associated to external loading. The equilibrium equation of each element layer in dynamics is obtained by adding inertia and damping forces contributions to the virtual work due to external loadings, which is given by Ref. [22]:

$$\Re^{t+\Delta t} = \sum_i \left(\int_V f_i^{B(t+\Delta t)}\ \delta u_i dV + \int_S f_i^{S(t+\Delta t)}\ \delta u_i dS - \int_V \rho\ \ddot{u}_i \delta u_i dV - \int_V \kappa\ \dot{u}_i \delta u_i dV \right) \tag{2}$$

where $f_i^{B(t+\Delta t)}$ and $f_i^{S(t+\Delta t)}$ are body and surface force components, respectively; ρ and κ are material mass density and damping parameters, respectively; $\ddot{u}_i$ and $\dot{u}_i$ are acceleration and velocity vector components, respectively; and δu_i is the corresponding virtual displacement vector component.

In Eq. (2), the third and the fourth terms in brackets result in element layer-k mass and damping matrices, respectively. Following the derivations of Aguiar et al. [2] the element kinematics of deformation, which is represented by Eq. (3), gives the displacement vector components of a point P, in a given layer-k, referred to the layer cross section reference system, as follows:

$$\begin{aligned}
u_P^k &= u^k - y\theta_z^k + z\theta_y^k + y\frac{\theta_x^k\theta_y^k}{2} + z\frac{\theta_x^k\theta_z^k}{2} \\
v_P^k &= v - z\theta_x^k - y\frac{\theta_x^{k2}+\theta_z^{k2}}{2} + z\frac{\theta_y^k\theta_z^k}{2} \\
w_P^k &= \underbrace{w + y\theta_x^k}_{\text{Linear}} \quad \underbrace{+y\frac{\theta_y^k\theta_z^k}{2} - z\frac{\theta_x^{k2}+\theta_y^{k2}}{2}}_{\text{Non-Linear}}
\end{aligned} \tag{3}$$

where u^k, v, w and θ_x^k, θ_y^k, θ_z^k are, respectively, the displacements and rotations of the geometric center of layer-k cross section; y and z are local coordinates of a point P referred to the layer-k cross section reference system.

Considering the element displacement field interpolation for a given layer-k, displacements within the element are interpolated, in the longitudinal direction, using Hermite polynomials, which represent straight beam linear solutions under constant normal, transverse shear and torsional internal loadings, for the Euler-Bernoulli beam model [2]. Thus, the displacement field at layer-k, results in:

$$
\begin{aligned}
u^k &= \underbrace{\left(1-\frac{\xi}{\ell}\right)u_1^k + \frac{\xi}{\ell}u_2^k}_{u_0^k} + \underbrace{\frac{6\phi_1}{\ell}y\nu_1 - \frac{6\phi_1}{\ell}y\nu_2}_{-\frac{dv_0}{d\xi}y} + \underbrace{\frac{6\phi_1}{\ell}zw_1 - \frac{6\phi_1}{\ell}zw_2}_{-\frac{dw_0}{d\xi}z} + \underbrace{\phi_2 z\theta_{y_1}^k - \phi_3 z\theta_{y_2}^k}_{\theta_y^k z} \\
&\quad + \underbrace{\left(-\phi_2 y\theta_{z_1}^k + \phi_3 y\theta_{z_2}^k\right)}_{-\theta_z^k y} + \underbrace{(1-6\phi_1)\,z\beta_1^k + (1-6\phi_1)\,y\beta_2^k}_{\beta_1^k \text{ and } \beta_2^k \text{ constants in } \xi} \\
v^k &= \underbrace{\phi_4\nu_1 + \phi_6\nu_2}_{v_0} + \underbrace{\left(-\left(1-\frac{\xi}{\ell}\right)z\theta_{x_1}^k - \frac{\xi}{\ell}z\theta_{x_2}^k\right)}_{-\theta_x^k z} + \underbrace{\phi_5\ell\theta_{z_1}^k - \phi_1\xi\theta_{z_2}^k}_{-\overline{v}^k} + (\xi-\phi_7\ell)\;\beta_2^k \\
w^k &= \underbrace{\phi_4 w_1 + \phi_6 w_2}_{w_0} + \underbrace{\left(1-\frac{\xi}{\ell}\right)y\theta_{x_1}^k + \frac{\xi}{\ell}y\theta_{x_2}^k}_{\theta_x^k y} + \underbrace{\left(-\phi_5\ell\theta_{y_1}^k + \phi_1\xi\theta_{y_2}^k\right)}_{\overline{w}^k} + (\xi-\phi_7\ell)\;\beta_1^k
\end{aligned}
\tag{4}
$$

where u_0^k is the axial displacements of the element centerline at layer-k; ℓ is the element length; ξ is the longitudinal coordinate along element ($0<\xi<\ell$); v_0 and w_0 are transverse displacements at the element centerline; $\overline{v}^k$ and $\overline{w}^k$ are transverse displacements along the layer-k centerline due to the nodal rotations θ_z^k e θ_y^k, respectively; and β_1^k and β_2^k are shear strains at planes $(\xi - y)$ and $(\xi - z)$, respectively (assumed constant along element length); and ϕ_i are the standard Hermite polynomials as defined in Ref. [2].

Equation (4) can be extended to element coordinates at layer-k as follows,

$$
\begin{bmatrix} u^k(\xi,\,y,\,z) \\ v^k(\xi,\,y,\,z) \\ w^k(\xi,\,y,\,z) \end{bmatrix} = \mathbf{H}(\xi,\,y,\,z)\,\mathbf{u}^k \tag{5}
$$

where $u^k(\xi,\,y,\,z)$, $v^k(\xi,\,y,\,z)$ and $w^k(\xi,\,y,\,z)$ are displacements at a point of local coordinates $(\xi,\,y,\,z)$, at the element layer-k; $\mathbf{H}(\xi,y,z)$ is the element interpolation matrix, defined as:

$$
\mathbf{H}(\xi,\,y,\,z) = \begin{bmatrix}
1-\frac{\xi}{\ell} & \frac{6y}{\ell}\phi_1 & \frac{6z}{\ell}\phi_1 & 0 & z\phi_2 & -y\phi_2 & \frac{\xi}{\ell} \\
0 & \phi_4 & 0 & -\left(1-\frac{\xi}{\ell}\right)z & 0 & \ell\phi_5 & 0 \\
0 & 0 & \phi_4 & \left(1-\frac{\xi}{\ell}\right)y & -\ell\phi_5 & 0 & 0
\end{bmatrix}
\begin{bmatrix}
-\frac{6y}{\ell}\phi_1 & -\frac{6z}{\ell}\phi_1 & 0 & -z\phi_3 & y\phi_3 & (1-6\phi_1)\,z & (1-6\phi_1)\,y \\
\phi_6 & 0 & -\frac{\xi}{\ell}z & 0 & -\xi\phi_1 & 0 & (\xi-\ell\phi_7) \\
0 & \phi_6 & \frac{\xi}{\ell}y & \xi\phi_1 & 0 & (\xi-\ell\phi_7) & 0
\end{bmatrix}_{3\times 14}
\tag{6}
$$

and $\mathbf{u}^k$ is the incremental displacement vector (nodal translations and rotations) associated to element layer-k, defined as:

$$\mathbf{u}^k = \left[u_1^k \quad v_1^k \quad w_1^k \quad \theta_{x_1}^k \quad \theta_{y_1}^k \quad \theta_{z_1}^k \quad u_2^k \quad v_2^k \quad w_2^k \quad \theta_{x_2}^k \quad \theta_{y_2}^k \quad \theta_{z_2}^k \quad \beta_1^k \quad \beta_2^k \right]^T \tag{7}$$

The element layers share the same axis, allowing slip between layers in axial and circumferential directions only. No gaps or separation between layers is included in the element formulation. The interaction between the axial and torsional degrees-of-freedom of two adjacent layers is driven by the interface stiffness matrix. However, the transverse displacements compatibility is not embedded in the formulation and must be imposed numerically. In the present work, this constraint condition is applied by using the penalty method as described in Ref. [2].

According to [2], the multilayered pipe beam element can be considered as "fully bonded" or "unbonded", depending on the type of interaction between layers. In the unbonded case, the element stiffness matrix is obtained by the regular FEM assembling process, accounting for the influence of each layer and interfaces and it's dimension is of order $14n_{layers} \times 14n_{layers}$ (n_{layers} is the number of layers in the element). In the fully bonded condition, there is no contribution of interface and penalty matrices, and the element matrix is obtained by simply adding all layer matrices. In this case the element matrix dimension is 14×14.

2.1. Element layer mass and damping matrices

The element mass and damping matrices are obtained by adding the contributions of each layer. At interface between layers the material is assumed to be very thin and its contribution to element mass and damping is assumed negligible. Mass and damping matrices associated to each element layer-k is obtained by substituting Eq. (5) into the inertia and damping terms of the expression for external forces work, given by Eq. (2), i.e.:

$$\int_{V^k} \rho^k \ddot{u}_i \delta u_i dV = \delta u \left(\int_{V^k} \rho^k \mathbf{H}^T \mathbf{H} dV \right) \ddot{\mathbf{u}}^k \quad \text{and} \quad \int_{V^k} \kappa^k \dot{u}_i \delta u_i dV = \delta u \left(\int_{V^k} \kappa^k \mathbf{H}^T \mathbf{H} dV \right) \dot{\mathbf{u}}^k \tag{8}$$

where $\dot{\mathbf{u}}^k$ and $\ddot{\mathbf{u}}^k$ are the layer-k nodal velocities and acceleration vectors, respectively.

Thus, the above equations furnish

$$\mathbf{M}^k = \int_0^{\ell} \int_{r_i^k}^{r_o^k} \int_0^{2\pi} r \, \rho^k \, \mathbf{H}^{k^T} \mathbf{H}^k \, d\varphi dr d\xi \quad \text{and} \quad \mathbf{D}^k = \int_0^{\ell} \int_{r_i^k}^{r_o^k} \int_0^{2\pi} r \, \kappa^k \, \mathbf{H}^{k^T} \mathbf{H}^k \, d\varphi dr d\xi \tag{9}$$

which are constant in this formulation.

Where $\mathbf{M}^k$ is the mass matrix associated to element layer k; $\mathbf{D}^k$ is the damping matrix for element layer k; $\mathbf{H}$ is the element interpolation matrix; ρ^k is the layer-k mass density; κ^k is the layer k material damping parameter; r_i^k and r_o^k are the inner and outer radii of layer k, respectively; and ℓ is the element length. In practice, the damping parameter (κ) is not readily available because damping properties are frequency dependent. For this reason, the matrix $\mathbf{D}^k$ is not obtained from Eq. (9). Here, the structure damping matrix is constructed from a linear combination of mass and stiffness matrices, as Rayleigh proportional damping [4].

3. Fluid loads

In a submerged pipeline various types of loadings due to internal and external fluid flows may occur, such as, internal fluid induced vibrations due to slugging flow and vortex induced vibrations, respectively. However, in this work only the internal fluid weight and hydrostatic (buoyancy) and hydrodynamic (drag forces) loads due to the external fluid are considered in the multilayered element

formulation. Since the effect of internal and external pressures in multilayered pipes is not straightforward, a simple approach, based on internal and external volumes, was used to obtain the hydrostatic and hydrodynamic loads acting on respective element layers. Fig. 1 shows the equivalent nodal forces in four possible relative positions of a two node pipe beam element in contact with the external fluid: (a) totally dry; (b) partially submerged with first node inside the fluid; (c) partially submerged with last node inside the fluid; and (d) totally submerged. Additionally, the following conditions may occur: open pipe, closed pipe with internal fluid and closed empty pipe.

3.1. Fluid weight and buoyancy forces

From equilibrium condition, the equivalent nodal forces due to internal fluid weight and external fluid buoyancy are obtained. Eq. (10) presents these equivalent nodal forces associated to each element layer (k), for the open and closed pipe conditions. Thus,

$$\begin{aligned} & F_1^k = \gamma_e A^k \ell \alpha_1 \quad \text{and} \quad F_2^k = \gamma_e A^k \ell \alpha_2 && \leftarrow \text{open} \\ & F_1^1 = -\frac{\gamma_i A_i \ell}{2}; \quad F_1^k = 0\left(1 < k < N_{layers}\right); \quad F_1^{N_{layers}} = \gamma_e A_e \ell \alpha_1 \\ & F_2^1 = -\frac{\gamma_i A_i \ell}{2}; \quad F_2^k = 0\left(1 < k < N_{layers}\right); \quad F_2^{N_{layers}} = \gamma_e A_e \ell \alpha_2 && \leftarrow \text{closed} \end{aligned} \tag{10}$$

where F_1^k, F_2^k are the layer-k equivalent nodal forces; γ_i , γ_e are the internal and external fluid densities, respectively; A_i, A_e are the internal and external areas, respectively; A^k is the layer-k cross section area; ℓ is the element length; and α_1, α_2 are coefficients to transfer the uniform distributed loads to element nodes, as given in Table 1.

Note that the internal and external areas, as well as the element length, are constant in this formulation. Thus, the equivalent nodal forces, due to internal fluid weight and external fluid pressure (buoyancy) are also constant.

3.2. Hydrodynamic loads

Fluid-structure interaction is generally characterized by drag and inertia (added mass) forces, obtained by using Morison's equation [20], which is a semi-empirical equation for the hydrodynamic forces on a cylinder in oscillatory flow. This equation can be used with confidence in structural analysis of risers, provided the pipe diameter is at least one order of magnitude small compared to the wavelength of the oscillatory flow. For a moving pipe in an oscillatory flow, Morison's equation is represented by three components as follows:

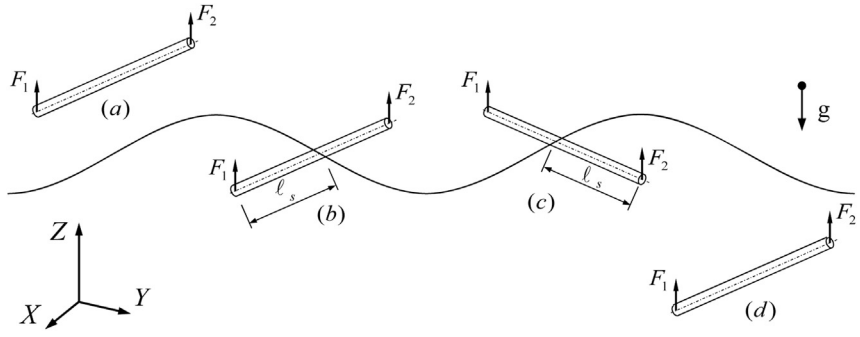

Fig. 1. Fluid load on a pipe beam element.

Table 1
Distributed loads proportional coefficients.

Element relative position	α_1	α_2
(a) Totally dry	0	0
(b) Partially submerged (node 1 inside fluid)	$\frac{\ell_s}{\ell}\left(1-\frac{\ell_s}{2\ell}\right)$	$\frac{1}{2}\left(\frac{\ell_s}{\ell}\right)^2$
(c) Partially submerged (node 2 inside fluid)	$\frac{1}{2}\left(\frac{\ell_s}{\ell}\right)^2$	$\frac{\ell_s}{\ell}\left(1-\frac{\ell_s}{2\ell}\right)$
(d) Totally submerged	$\frac{1}{2}$	$\frac{1}{2}$

Where ℓ_s is the pipe submerged length as shown in Fig. 1.

(1) Transverse drag forces:

$$\mathbf{f}_{Dn} = \frac{1}{2}\rho_f D C_{Dn}\left|\dot{\mathbf{u}}_{fn} - \dot{\mathbf{u}}_n\right|\left(\dot{\mathbf{u}}_{fn} - \dot{\mathbf{u}}_n\right) \tag{11}$$

(2) Tangential drag forces:

$$\mathbf{f}_{Dt} = \frac{1}{2}\rho_f D C_{Dt}\left|\dot{\mathbf{u}}_{ft} - \dot{\mathbf{u}}_t\right|\left(\dot{\mathbf{u}}_{ft} - \dot{\mathbf{u}}_t\right) \tag{12}$$

(3) Transverse inertia forces:

$$\mathbf{f}_I = \rho_f \frac{\pi D^2}{4} C_M \ddot{\mathbf{u}}_{fn} - \rho_f \frac{\pi D^2}{4}(C_M - 1)\ddot{\mathbf{u}}_n \tag{13}$$

where ρ_f is the fluid mass density; D is the hydrodynamic diameter of the pipe; C_{Dn} and C_{Dt} are the normal and tangential drag coefficients, which depend on the pipe cross section geometry and roughness (for a bare cylinder: $C_{Dn} = 1.0$ and $C_{Dt} = 0.0$); C_M is the transverse inertia coefficient; $\dot{\mathbf{u}}_{fn}$ and $\dot{\mathbf{u}}_n$ are the fluid and structure velocity vectors, respectively, both normal to the pipe centerline; $\dot{\mathbf{u}}_{ft}$ and $\dot{\mathbf{u}}_t$ are the fluid and structure velocity vectors, respectively, in the pipe tangential direction; $\ddot{\mathbf{u}}_{fn}$ and $\ddot{\mathbf{u}}_n$ are the fluid and structure acceleration vectors, respectively, both normal to the pipe centerline.

The total hydrodynamic load per unit length is the vector sum of Eqs. (11)–(13) along the element axis. In the multilayered element formulation, the nodal equivalent hydrodynamic forces are obtained assuming a linear variation along the length, i.e.:

$$\mathbf{f}_h(\xi) = \left(1 - \frac{\xi}{\ell}\right)\mathbf{f}_h^1 + \left(\frac{\xi}{\ell}\right)\mathbf{f}_h^2 \tag{14}$$

where $\mathbf{f}_h^1$ and $\mathbf{f}_h^2$ are the hydrodynamic load per unit length at nodes 1 and 2, respectively; ξ is the local coordinate along element axis; and ℓ is the element length.

The distributed loading in Eq. (14) is then transferred to the external layer nodes, by using the element interpolation matrix, i.e.:

$$\mathbf{F}_h = \int_0^{\ell} \mathbf{H}^T \mathbf{f}_h d\xi \tag{15}$$

where $\mathbf{F}_h$ is the nodal vector of hydrodynamic loads applied to the external layer.

4. Implementation of the three-dimensional multilayer element

The three-dimensional multilayered element formulation has been implemented in a C++ code using object-oriented techniques, such as proposed by Lages et al. [16]. The program uses some of the

nonlinear solution algorithms presented by Leon et al. [17], together with the HHT time integration algorithm (Hilber et al. [13]), to solve the resulting nonlinear dynamic equilibrium equations.

4.1. Global equilibrium equation

The present formulation includes large displacements and nonlinear constitutive relations within the interface material. Numerical solutions are obtained using an incremental procedure for equilibrium. The global dynamic equilibrium equation is presented in the following matrix form:

$$\mathbf{M}\,{}^{t+\Delta t}\ddot{\mathbf{U}} + \mathbf{D}\,{}^{t+\Delta t}\dot{\mathbf{U}} + {}^{t+\Delta t}\mathbf{K}\,\Delta\mathbf{U} = {}^{t+\Delta t}\mathbf{R} - {}^{t}\mathbf{F} \tag{16}$$

where $\mathbf{M}$ and $\mathbf{D}$ are the structure global mass and damping matrices, obtained from the elements matrices in Eq. (9), through an assemblage process; ${}^{\mathbf{t}+\Delta t}\mathbf{K}$ is the updated structure global stiffness matrix, obtained from the elements matrices [2] through an assemblage process; ${}^{\mathbf{t}+\Delta t}\ddot{\mathbf{U}}$ and ${}^{\mathbf{t}+\Delta t}\dot{\mathbf{U}}$ are the updated global nodal acceleration and velocities vectors; $\boldsymbol{\Delta U}$ is the global incremental displacements vector; ${}^{\mathbf{t}+\Delta t}\mathbf{R}$ is the updated global external loading vector; and ${}^{t}\mathbf{F}$ is the structure global unbalanced internal forces vector at time t.

A step-by-step procedure has been implemented considering

$$\begin{aligned}
{}^{t+\Delta t}\ddot{\mathbf{U}} &= \frac{1}{\beta\Delta t^2}\Delta\mathbf{U} - \frac{1}{\beta\Delta t}\,{}^{t}\dot{\mathbf{U}} - \left(\frac{1}{2\beta} - 1\right){}^{t}\ddot{\mathbf{U}} \\
{}^{t+\Delta t}\dot{\mathbf{U}} &= {}^{t}\dot{\mathbf{U}} + (1-\gamma)\Delta t\,{}^{t}\ddot{\mathbf{U}} + \gamma\Delta t\,{}^{t+\Delta t}\ddot{\mathbf{U}} \\
{}^{t+\Delta t}\mathbf{U} &= {}^{t}\mathbf{U} + \Delta\mathbf{U}
\end{aligned} \tag{17}$$

where Δt is the time increment; ${}^{t}\mathbf{U}$ is a known solution at time t; β and γ are constants that define the time integration algorithm. In the case of HHT

$$\beta = \frac{1}{4}(1-\alpha)^2 \quad \text{and} \quad \gamma = \frac{1}{2} - \alpha, \quad -1/3 \le \alpha \le 0. \tag{18}$$

5. Numerical tests

The multilayer pipe beam element formulation has been implemented in a computer program and a number of analyses were carried out to verify the element performance in representing the behavior of risers in statics as well as in dynamics. In the next sub-sections, the following examples are presented:

- Two-Layer Cantilever Beam Subjected to Distributed Loading;
- Dynamic Analysis of a Circular Two-Layer Cantilever Beam;
- Two-Layer Cantilever Under Hydrostatic and Hydrodynamic Loading;
- Flexible Riser in Catenary Configuration;
- Multilayered Steel Catenary Riser;

5.1. Two-layer cantilever beam subjected to distributed loading

The objective of this analysis is to test the multilayered pipe beam element under large displacement in static and dynamic loadings. The model was originally proposed by Bathe and Bolourchi [3] for the representation of 3D beams in large displacement analysis. In this analysis a two-layer cantilever pipe beam under a uniformly distributed load was considered, as shown in Fig. 2. The beam is modeled using 8 equally spaced elements with the load applied in the internal layer nodes, as in a pipe with internal fluid.

Static solution for the vertical displacement at the beam tip was obtained with applied load in 20 equal increments. As shown in Fig. 3, numerically obtained results are in good agreement with the

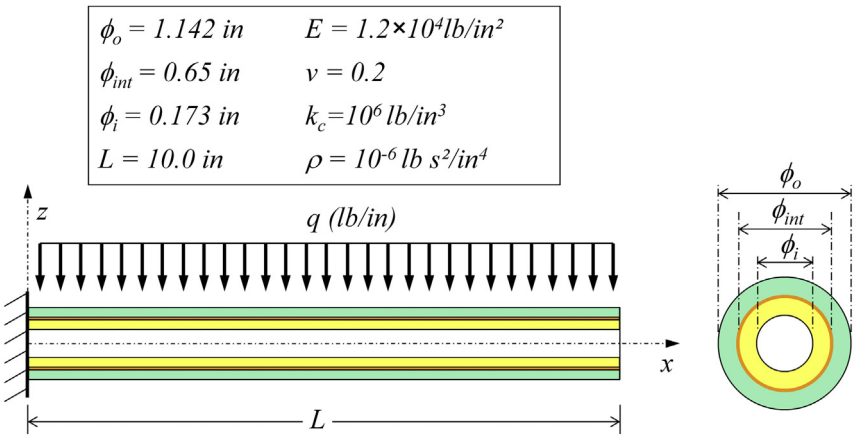

Fig. 2. Properties for the two-layer cantilever beam under distributed loading.

solution given in Bathe and Bolourchi [3]. Because a very high interlayer contact parameter (k_c) was considered [2], vertical displacements at both layers are supposed to be equal, and thus, only inner layer results are presented in Fig. 3.

The dynamic analysis was performed with a step uniform loading $q = 2.85\ lb/in$. A total time analysis of $1.215 \times 10^{-2}\ s$ was used, with time increments of $\Delta t = 1.35 \times 10^{-4}\ s$. The dynamic response for the vertical displacements at the tip of the beam inner layer is presented in Fig. 4, obtained using the HHT time integration algorithm along with the Newton–Raphson iterative scheme. As shown, the dynamic response in Bathe and Bolourchi [3] presents some damping effects, without any further information provided. Thus, considering a damping coefficient equals to 1.0%, proportional to the element stiffness, as in the Rayleigh proportional damping [4], the model analysis provides a better agreement for the beam transverse displacement results, as shown in Fig. 4.

5.2. Dynamic analysis of a circular two-layer cantilever beam

This example has been studied by several authors such as Crisfield [8], Bathe and Bolourchi [3], Simo and Vu-Quoc [26] and Cardona and Geradin [1] in the evaluation of 3D general beams in statics. It

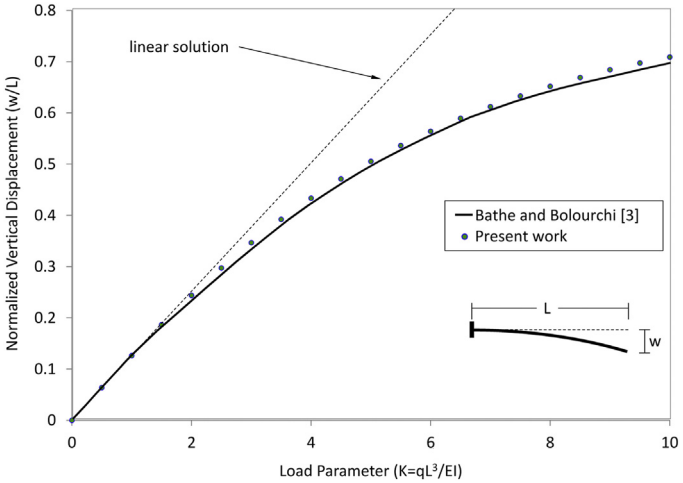

Fig. 3. Beam tip displacements in static analysis.

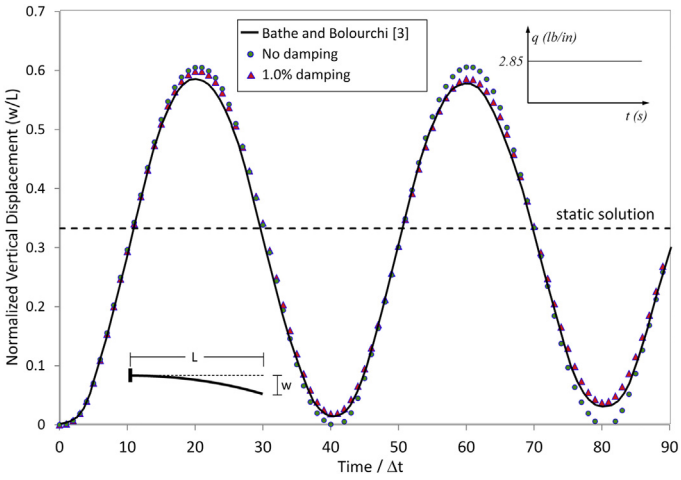

Fig. 4. Beam tip displacements – dynamic analysis.

presents a very useful testing to full 3D non-linear behavior of beam elements, including bending, torsion and transverse shear. The beam consists of a curved pipe over 45°, with 100 *m* constant radius and under transverse loading, as shown in Fig. 5. In the present study, the circular cantilever beam is considered with a two-layer cross section displaying the same material properties and a very high interlayer contact parameter (k_c) to represent the original homogeneous beam. The numerical analysis intends to evaluate the performance of the multilayered element in 3D large displacement dynamic analysis. This model was analyzed under dynamic loading by Chan [7], using the conventional homogeneous pipe beam formulation. The tip displacements, resulting from a suddenly applied load equal to 300 *lb* are plotted in Fig. 6 for a total time of 0.3 *s*, with a time increment $\Delta t = 0.002$ *s* used. Fig. 6 shows good agreement between the two-layered pipe beam displacement results and the ones obtained by Chan [7].

The same beam has also been studied with two different materials ($E_i = 2E_o = 10^7$ *psi* and $\rho_i = \rho_o = 2.54 \times 10^{-6}$ *lb* s^2/in^4), for the inner and outer layer, respectively. The time history results for

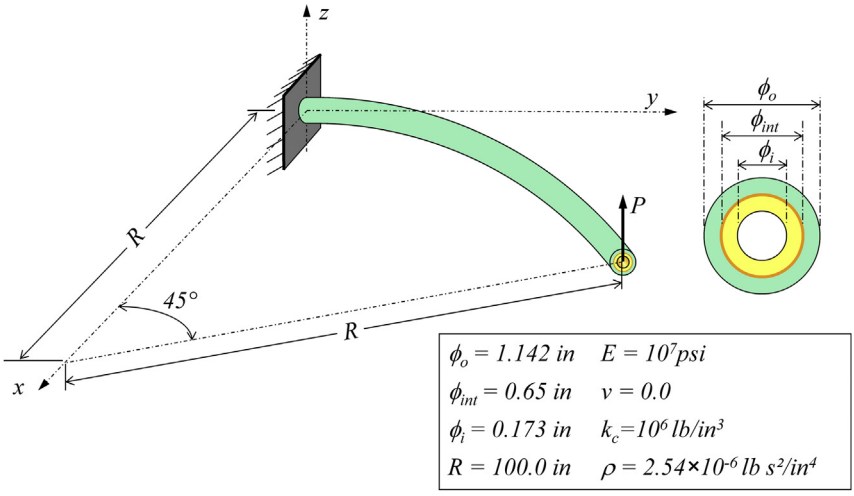

Fig. 5. Geometrical and material properties for the circular two-layer cantilever pipe beam.

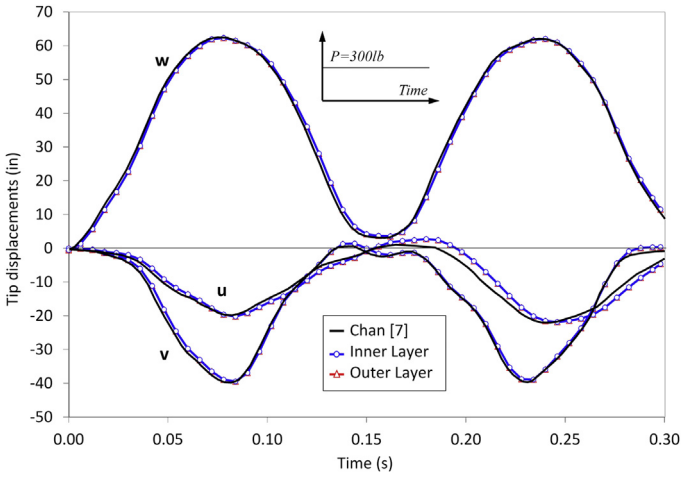

Fig. 6. Circular cantilever pipe beam tip displacements – single material.

vertical movements, at beam tip, are shown in Fig. 7. These results show that the dynamic response of the beam is substantially modified when different materials are used.

5.3. Two-layer cantilever under hydrostatic and hydrodynamic loading

A two-layer submerged capped ends cantilever pipe, under vertical concentrated load at the free end is considered. The objective of this analysis is to verify the behavior of the multilayer pipe beam element under gravity loading combined with external and buoyancy loads. This study was carried out by Yazdchi and Crisfield [29] using a 2D pipe beam formulation in static analysis. The material and geometrical properties are shown in Fig. 8.

The beam was represented using a 20 equal element model under concentrate loadings applied to the internal layer node. Static deformed configurations obtained for four loading conditions are shown in Fig. 9, which are in very good agreement with the ones presented by Yazdchi and Crisfield [29]. In dynamic analysis, a total time of 30 *s* was considered for a constant time increment of 0.1 *s*. In the numerical analysis an upward load was statically applied to the submerged beam and suddenly

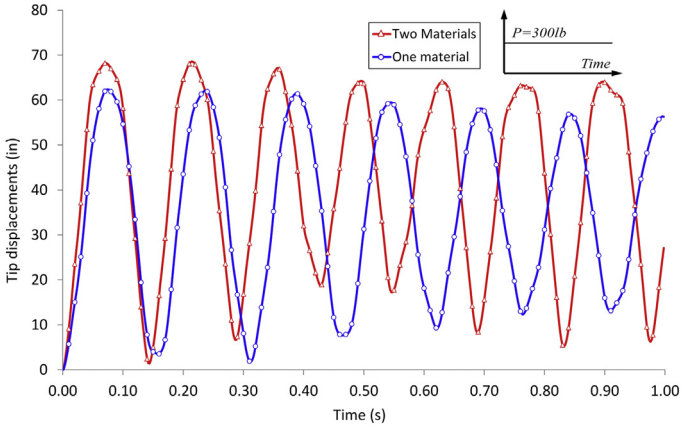

Fig. 7. Circular cantilever pipe beam vertical tip displacements – two materials.

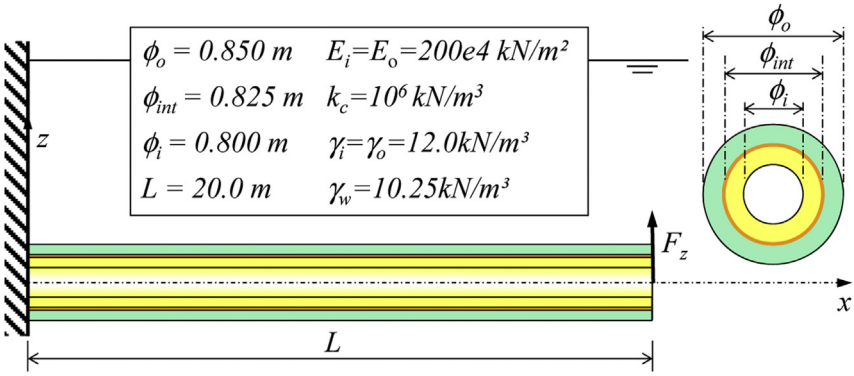

Fig. 8. Submerged cantilever beam.

removed. Results for vertical displacements at the beam tip are shown in Fig. 10, where hydrodynamic damping effects are noticeable. Besides, this plot also includes results for a beam with different materials ($E_i = 2E_o = 400e4 kN/m^2$ and $\gamma_i = \gamma_o = 24\ kN/m^3$) in each layer. As shown, obtained results for the single material two layer pipe beam are in good agreement with the conventional homogeneous beam solution.

5.4. Flexible riser in catenary configuration

In this example a 350.0 *m* long flexible catenary riser is considered. In the setup, the riser is connected, at the top, to a floating unit and at the bottom to a sub-sea tower, at a water depth of 150.0 *m*, which is horizontally displaced 150.0 *m* from the top connection. The riser is assumed to be filled with seawater. The finite element mesh employed 16 equal 20.0 *m* elements, two 10.0 *m* elements and two 5.0 *m* long elements. Geometric, material and hydrodynamic properties used in the model, as well as details of the finite element mesh used, are shown in Fig. 11. Analysis of this riser system has been reported by McNamara et al. [19], Yazdchi and Crisfield [30], Kordkheili et al. [14].

The riser was modeled with three layers considering the properties shown in Table 2. A flexible riser is a composite construction of interlocked steel and polymeric layers designed to give the structure an axial stiffness approximately five orders of magnitude greater than the bending stiffness. Thus, to

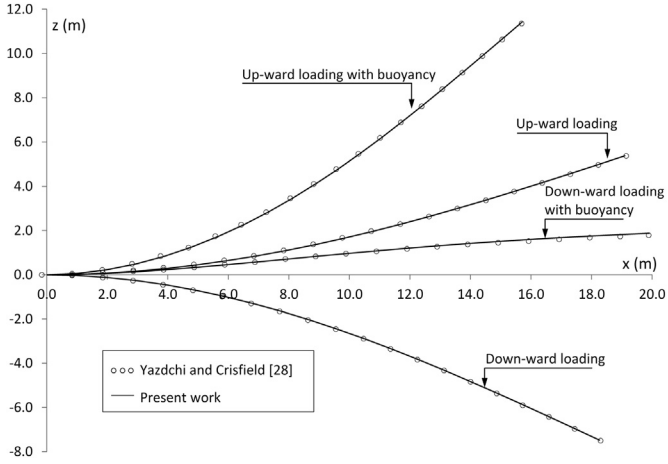

Fig. 9. Cantilever beam deformed shapes for various loading conditions.

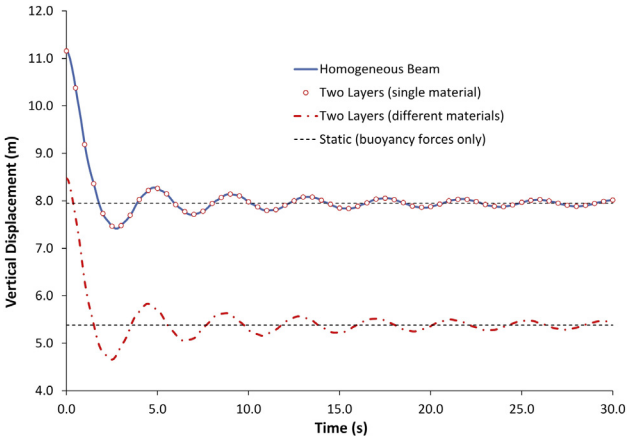

Fig. 10. Vertical displacements at beam tip.

reproduce the stiffness properties presented in Fig. 11, the numerical model was modified to consider a stiffening factor (*EA/EI*) in all layers.

A dynamic analysis has been carried out considering self-weight, buoyancy forces and prescribed displacement at the top node due to ship motion. A horizontal harmonic excitation with amplitude of 2.01 *m* and a corresponding period of 14.0 *s* was considered. The results of this analysis are shown in Fig. 12 and compared to the solution obtained by Yazdchi and Crisfield [30]. The vertical reaction at both the top and bottom nodes are in good agreement with their solutions.

5.5. Multilayered Steel Catenary Riser

This example reflects a real case scenario, considering a 4000 *m* long steel catenary riser (SCR) is considered. Installed in a water depth of 2220 *m*, the riser is connected to a floating production unit (FPU) 15 *m* below the still water level (SWL) with a hang-off angle of 17°, as shown in Fig. 13. A uniform finite element mesh with one thousand elements is used to model the SCR, with the top connection node assumed free to rotate while the bottom connection node is kept fixed.

The riser cross section is a carbon-steel pipe with a corrosion resistant alloy (CRA - clad or liner) as inner layer and two external layers of syntactic and solid polypropylene for thermal insulation.

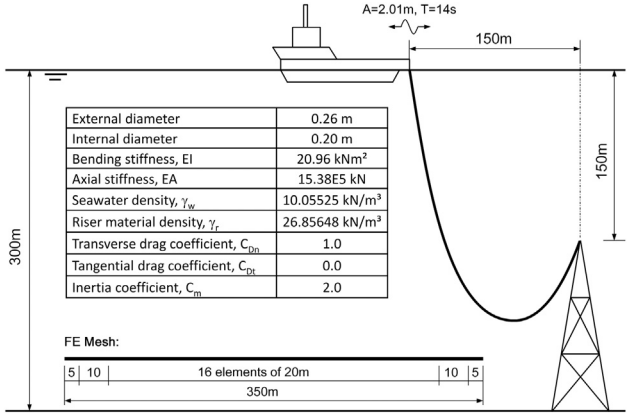

Fig. 11. Flexible riser in catenary configuration.

Table 2
Multilayer riser properties.

Internal diameter, D_i	0.20 m
External diameter, D_o	0.26 m
Inner layer thickness, t_i	0.003 m
Middle layer thickness, t_m	0.024 m
Outer layer thickness, t_o	0.003 m
Inner layer Young modulus, E_i	6.76E+05 kN/m^2
Middle layer Young modulus, E_m	6.76E+03 kN/m^2
Outer layer Young modulus, E_o	6.76E+05 kN/m^2
Inner layer density, γ_i	129.12 kN/m^3
Middle layer density, γ_m	1.2912 kN/m^3
Outer layer density, γ_o	129.12 kN/m^3
Stiffening factor, (EA/EI)	7.3378E+04
Contact stiffness, k_c	1.0E+06 kN/m^3

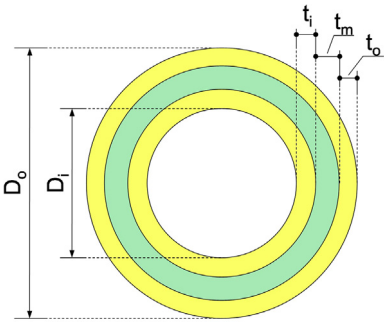

multilayered riser cross section

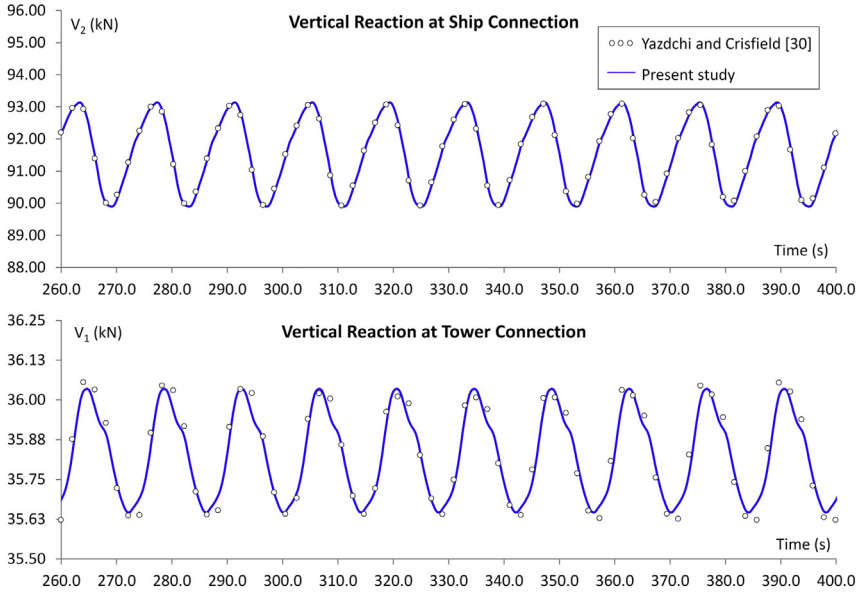

Fig. 12. Dynamic analysis results for multilayered flexible riser.

Dimensions and material properties of each layer cross section are shown in Table 3, while details on layer arrangements are shown in Fig. 14.

Nonlinear springs attached to the element nodes are used to represent vertical contact and friction reactions in longitudinal and lateral directions, at the seabed surface, which is assumed horizontal. The soil springs properties are shown in Table 4.

Static and dynamic analyses have been carried out considering self-weight, buoyancy forces, prescribed displacements at the top connection and a current profile along the water depth. In the static analysis, a horizontal prescribed displacement of 111 *m* (5% of water depth) was applied to the top node, aligned with the current profile, in a direction 45° from the XZ plane, as shown in Fig. 15. The current profile is assumed linear, varying from 0.2 *m/s* at seabed to 1.2 *m/s* at the sea surface. The static analysis was performed with 21 load increments. In the first load increment, only self-weight and

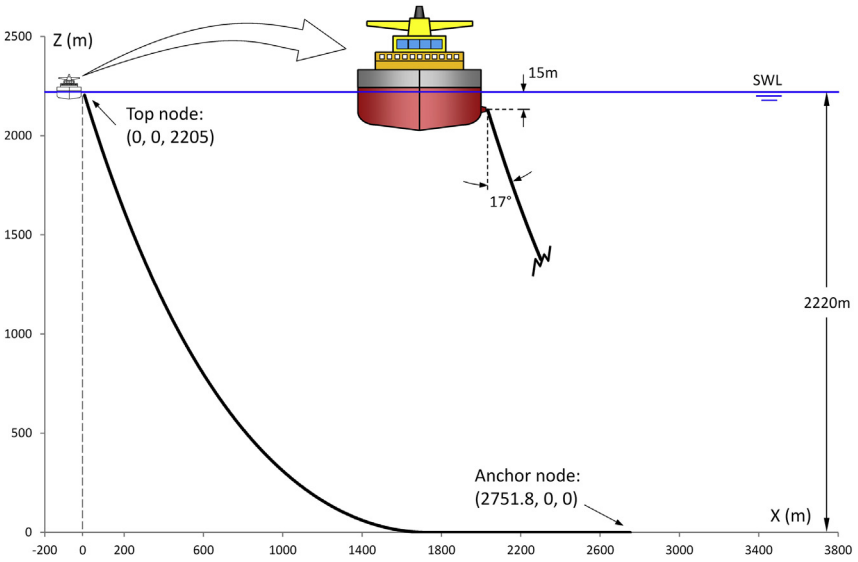

Fig. 13. Initial deformed configuration for the steel catenary riser.

Table 3
Multilayered SCR cross section properties.

	CRA	Steel	Syntactic PP	Solid PP
Structural external diameter, D_i (m)	0.185	0.225	0.375	0.387
Structural internal diameter, D_o (m)	0.175	0.185	0.225	0.375
Pipe internal diameter, D_i (m)	0.175	0.175[a]	–	–
Layer thickness, t_i (m)	0.005	0.020	0.075	0.006
Young modulus, E (kN/m^2)	1.96E08	2.07E08	1.08E06	1.30E06
Material density, γ (kN/m^3)	79.853	77.000	6.278	8.829
Inertia coefficient, CM	–	2.0[a]	–	2.0
Drag coefficient, CD	–	1.0[a]	–	1.0
Contact stiffness, k_c (kN/m^3)[b]	1.00E03	1.00E06	1.00E06	
Hydrodynamic diameter (m)	–	0.387[a]	–	0.387
Internal/External coating weight (kN/m)	–	0.73295[a]	–	–
Internal/External coating buoyancy (kN/m)	–	0.78298[a]	–	–

[a] Values used in the single layer homogeneous pipe only.
[b] Values used in the unbonded multilayer model only.

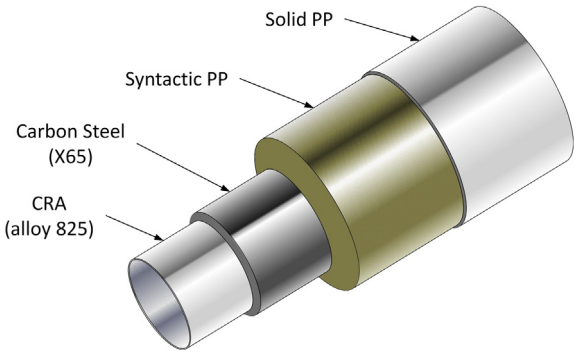

Fig. 14. SCR pipe cross section.

Table 4
Soil properties for the SCR model.

Longitudinal elastic limit, u_{lx} (m)	0.030
Lateral elastic limit, u_{ly} (m)	0.219
Longitudinal friction coefficient, μ_x	0.71
Lateral friction coefficient, μ_y	0.73
Normal spring stiffness, k_n (kN/m)	987.0

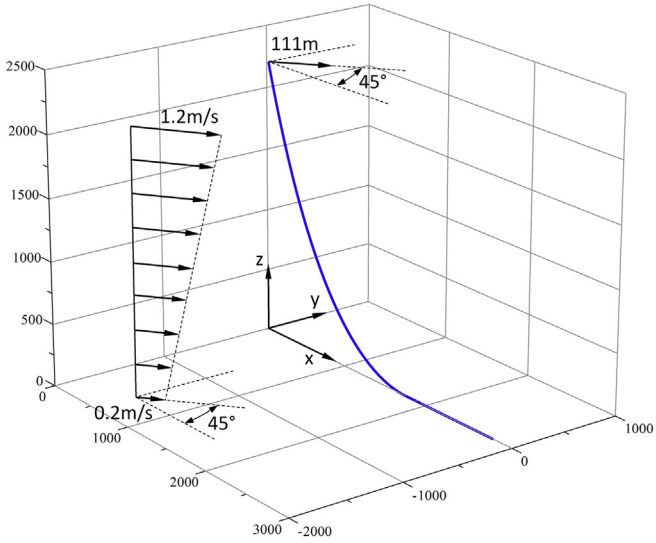

Fig. 15. Static loading for the SCR model.

buoyancy forces were applied in the model, while prescribed displacement and current loading were applied simultaneously in the following 20 load increments.

The dynamic analysis was carried out using the final static configuration as initial condition with all static loading kept constant during dynamic simulation. A harmonic excitation was considered in the *XZ* plane with amplitudes of 3.4 *m* and 5.1 *m* in *X* and *Z* directions, respectively, and period of 11.2 *s*. Fig. 16 shows the displacement history applied to the riser's top connection during the total dynamic analysis simulation time of 70 *s* in 700 equal time increments.

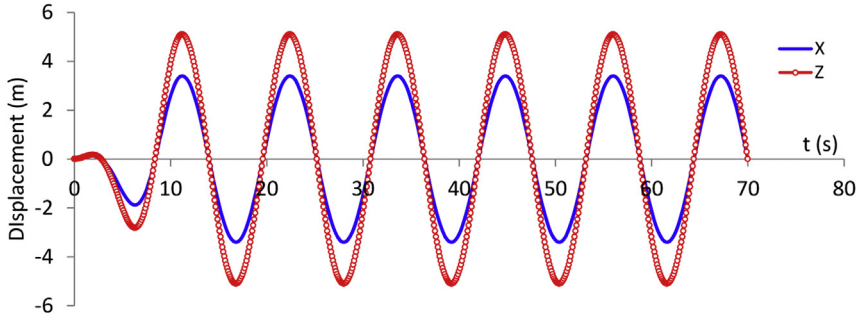

Fig. 16. Dynamic loading for the SCR model.

In the analysis of the SCR, three distinct models were considered: single layer homogeneous beam, bonded multilayer beam (cladded pipe) and unbonded multilayer beam (lined pipe). In the first model, only the carbon steel layer is considered, while the stiffness of the remaining layers was neglected. This is a common assumption employed in global riser analysis. In this case, CRA and thermal insulation layers are considered for weight, buoyancy and drag load evaluations only. In the multilayered models however, all layers are modeled in a discrete fashion. The deformed configuration at the end of static analysis is essentially the same in all model analysis. It is compared to the initial deformed configuration in Fig. 17.

Results from the static analysis for axial forces, bending moments and stresses at the top connection and touchdown point (TDP) are shown in Table 5.

The stresses in Table 5 are the maximum values between the in-plane and out-of-plane stresses. They were calculated at the external layer wall, by means of the following expressions:

$$
\begin{aligned}
\sigma_{vM} &= \sqrt{(\sigma_{11}-\sigma_{22})^2+(\sigma_{22}-\sigma_{33})^2+(\sigma_{33}-\sigma_{11})^2+6\left(\sigma_{12}^2+\sigma_{13}^2\right)}\\
\sigma_{11} &= \frac{N}{A}+\frac{Mr}{I}+\frac{p_i r_i^2-p_o r_o^2}{r_o^2-r_i^2}, \quad M=M_y \text{ or } M_z\\
\sigma_{22} &= \frac{p_i r_i^2-p_o r_o^2}{r_o^2-r_i^2}-\frac{r_i^2 r_o^2(p_o-p_i)}{r^2\left(r_o^2-r_i^2\right)}\\
\sigma_{33} &= \frac{p_i r_i^2-p_o r_o^2}{r_o^2-r_i^2}+\frac{r_i^2 r_o^2(p_o-p_i)}{r^2\left(r_o^2-r_i^2\right)}\\
\sigma_{12} &= \frac{4V}{3A}+\frac{M_x r}{J}, \quad V=V_y \text{ or } V_z\\
\sigma_{13} &= \frac{4V}{3A}, \qquad\qquad V=V_z \text{ or } V_y
\end{aligned}
\tag{19}
$$

where σ_{vM} is the von Mises equivalent stress; M_x is the torsion moment, M_y and M_z are the bending moments in y and z directions, respectively; V_y and V_z are the shear forces in y and z directions,

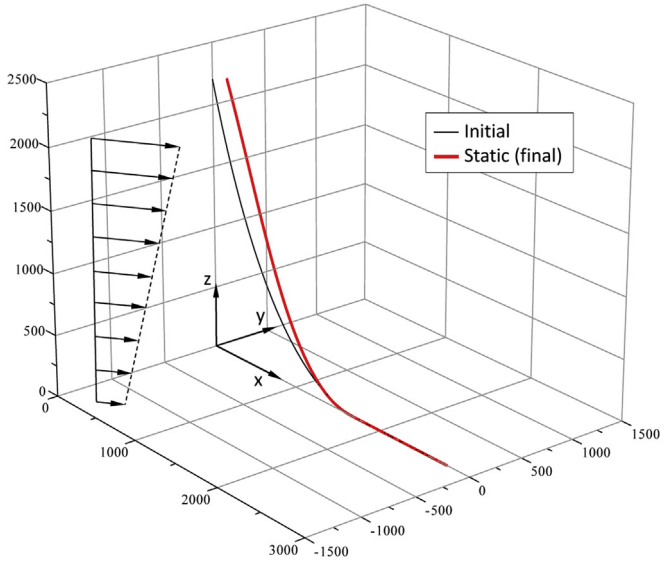

Fig. 17. Deformed configuration at the end of static analysis.

Table 5
SCR static analysis numerical results.

Model	Self-weight and buoyancy			Self-weight, buoyancy, prescribed displacement and current		
	Axial force at top (kN)	Bending Moment at TDP (kN·m)	von Mises stress at TDP (MPa)	Axial force at top (kN)	Bending Moment at TDP (kN·m)	von Mises stress at TDP (MPa)
Homogeneous (Steel)	2134.87	15.56	83.12	1965.70	21.34	77.52
Bonded multilayer						
Sum	2139.52	19.20	–	1970.12	26.32	–
CRA	359.06	2.47	144.31	330.66	3.38	143.27
Steel	1722.53	15.54	72.36	1585.93	21.30	71.37
Syntactic PP	50.59	1.00	–	46.67	1.37	–
Solid PP	7.34	0.19	–	6.85	0.26	–
Unbonded multilayer						
Sum	2142.02	19.18	–	1972.46	26.29	–
CRA	358.92	2.47	144.31	331.84	3.38	143.26
Steel	1724.77	15.53	72.38	1586.75	21.28	71.36
Syntactic PP	50.16	1.00	–	46.21	1.37	–
Solid PP	8.17	0.19	–	7.67	0.26	–

respectively; A, I and J are the layer cross section area, moment of inertia and polar moment of inertia, respectively; r_i and r_o are the layer cross section inner and outer radius, respectively; p_i and p_o are the internal and external pressures in the pipe, respectively; and r is radius to the point where the stresses are calculated ($r_i \leq r \leq r_o$).

Envelopes for axial forces, bending moments and von Misses stresses along the line, from the dynamic analysis of the bonded multilayered model, are shown in Figs. 18–20. Note that the stresses (Fig. 20) at TDP are very similar for homogeneous and multilayered models, but they are quite different at the top of the riser: at TDP, bending moment (Fig. 19) contributions to stresses are predominant, while at the top, the axial forces (Fig. 18) have more influence in stresses.

Results obtained for the unbonded multilayered model are also compared to the homogeneous beam results in Figs. 21–22. Bonded and unbonded multilayered beam solutions are very similar.

Time history for the axial forces at top connection and the bending moment at TDP are shown in Figs. 23 and 24, respectively. These results show that the homogeneous beam model lead to conservative values for axial forces at the top of the riser.

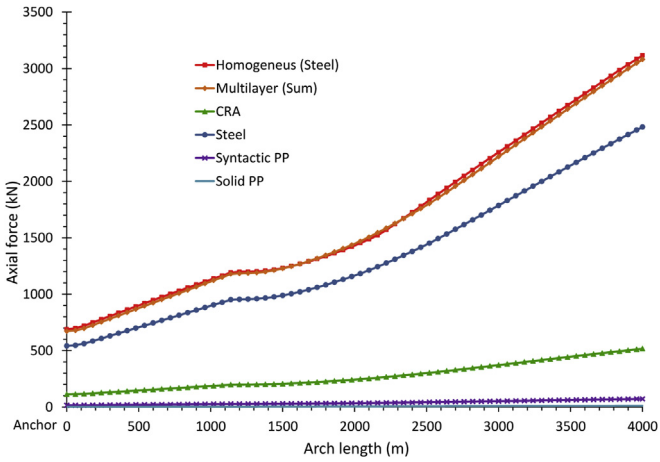

Fig. 18. Axial forces envelope – Bonded Model.

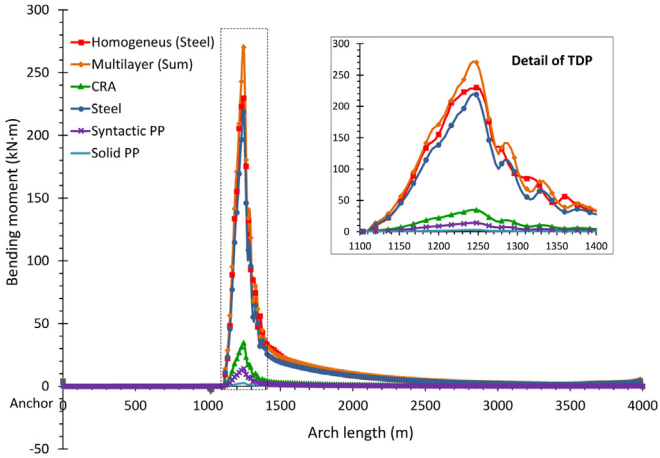

Fig. 19. Bending moment envelope – Bonded and Unbonded Models.

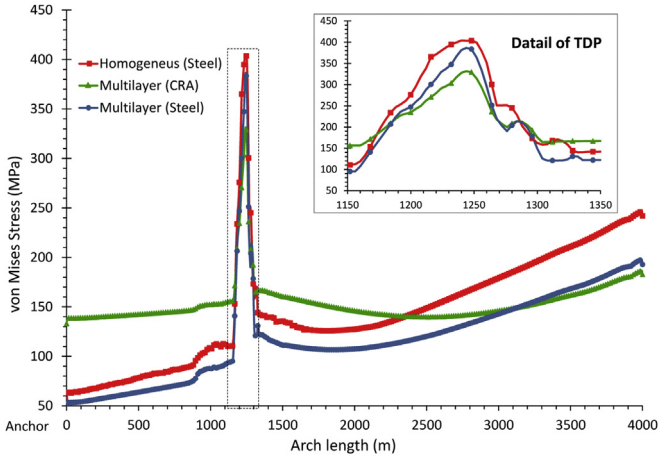

Fig. 20. von Mises stress envelope – Bonded Model.

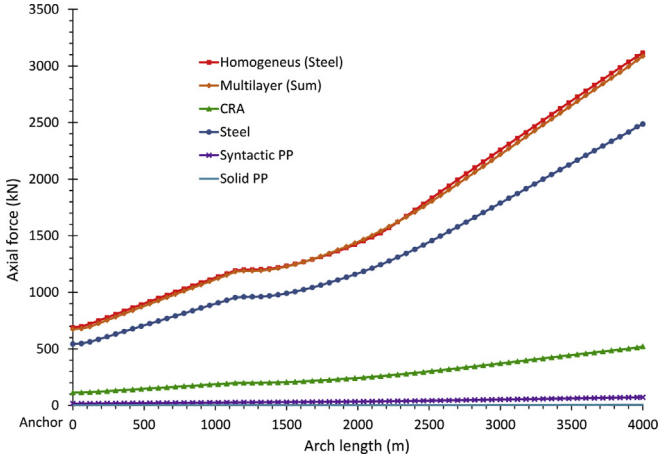

Fig. 21. Axial forces envelope – Unbonded Model.

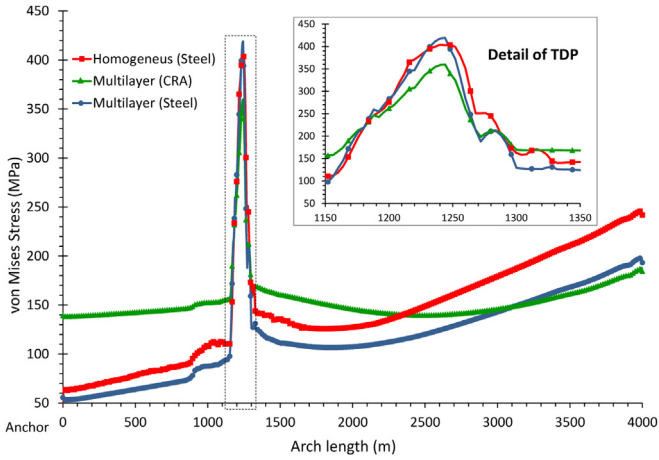

Fig. 22. von Mises stresses envelope – Unbonded Model.

6. Concluding remarks

A new finite element formulation for nonlinear dynamic analysis of multilayered pipes has been presented. The formulation is capable of an accurate and detailed representation of multilayered pipes in large displacement and rotation analyses. Hydrostatic and hydrodynamic loadings, due to the internal and external fluids acting on each layer corresponding degrees-of-freedom are derived in a simple way, without considering the effect of internal and external pressures. Numerical test results are in very good agreement with the solutions available in the literature. Additionally, the element provides detailed results for stresses and internal forces of each element layer. Applications to riser analysis show very little influence of the detailed multilayer representation in the global dynamic response of the riser. However, the solution results show that the homogenous model assumption may lead to conservative values for stresses and axial forces at the top of the riser. The FE implementation is very robust and efficient, even for large scale riser analysis, as shown by the numerical examples presented.

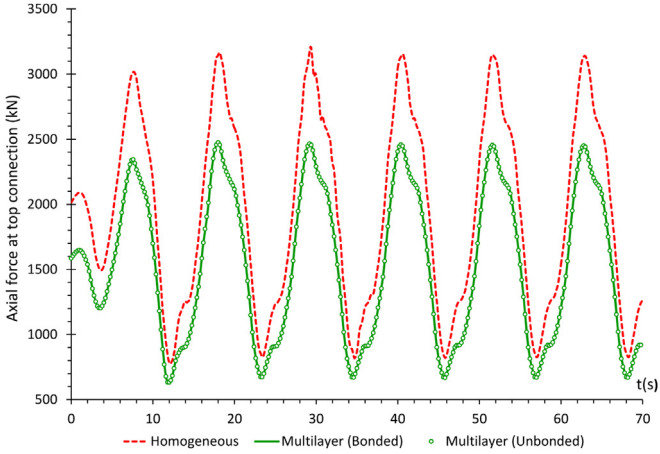

Fig. 23. Time history for axial force at top connection.

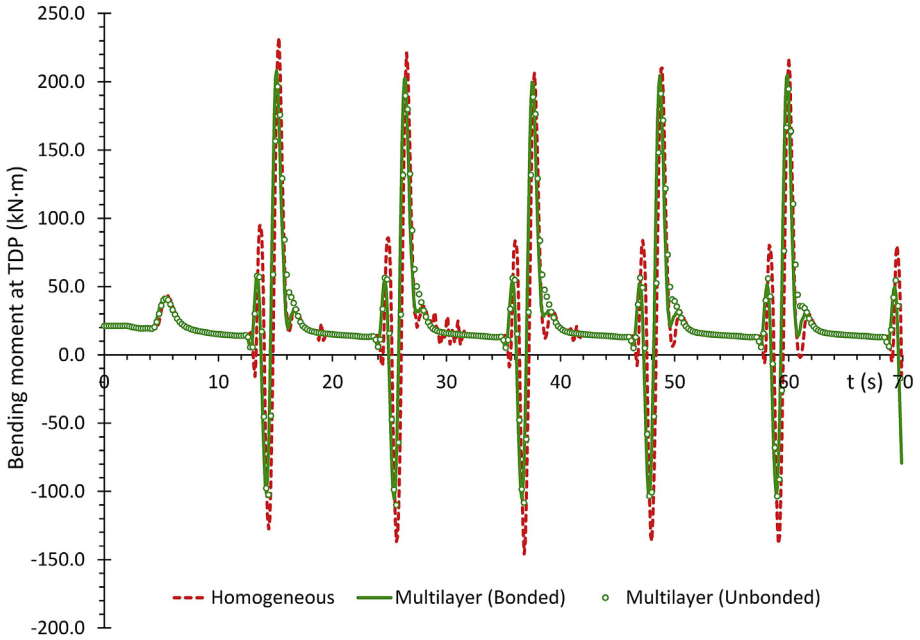

Fig. 24. Time history for bending moment at touchdown point (TDP).

Acknowledgments

Aguiar, L. L. thanks the financial support provided by PETROBRAS – Petroleo Brasileiro S.A. and Pontifical Catholic University of Rio de Janeiro that made this doctoral research possible.

Appendix A. Nomenclature

i	vector index; node index; iteration;
k	element layer index;
t	time;
$X,\ Y,\ Z$	local element reference system;
$x,\ y,\ z$	nodal reference system; local coordinates on element cross section;
ξ	element coordinate in the longitudinal (X) direction;
ℓ	element length;
N_{layers}	number of layers;
$\mathbf{u}$	displacement vector;
$\dot{\mathbf{u}}$	velocities vector;
$\ddot{\mathbf{u}}$	acceleration vector;
u, v, w	components of displacements in the X, Y and Z directions, respectively;
$\theta_x, \theta_y, \theta_z$	components of rotations about X, Y and Z axis, respectively;
β	generalized degree-of-freedom for shear strain;
ρ	mass density;
$\mathbf{H}$	interpolation matrix;
$\mathbf{K}$	stiffness matrix;
$\mathbf{M}$	mass matrix;
$\mathbf{D}$	damping matrix;
$\mathbf{R}$	external forces vector;

$\mathbf{F}$	internal forces vector;
k_c	contact stiffness between layers (slip modulus);
A^k	layer k cross section area;
A_i	pipe internal area;
A_e	pipe external area;
γ_i	internal fluid density;
γ_e	external fluid density;
ℓ_s	submerged length;

References

[1] Cardona A, Geradin M. A beam finite element non-linear theory with finite rotations. Int J Numer Methods Eng 1988; 26(11):2403–38.
[2] Aguiar LL, Almeida CA, Paulino GH. A three-dimensional multilayered pipe beam element: nonlinear analysis. Comput Struct 2014;138 c:142–61.
[3] Bathe KJ, Bolourchi S. Large displacement analysis of three-dimensional beam structures. Int J Numer Methods Eng 1979; 14(7):961–86.
[4] Bathe KJ. Finite element procedures. New Jersey: Prentice-Hall; 1996.
[5] Čas B, Saje M, Planinc I. Buckling of layered wood columns. Adv Eng Softw 2007;38(8–9):586–97.
[6] Čas B, Saje M, Planinc I. Non-linear finite element analysis of composite planar frames with an interlayer slip. Comput Struct 2004;82(23–26):1901–12.
[7] Chan SL. Large deflection dynamic analysis of space frames. Comput Struct 1996;58(2):381–7.
[8] Crisfield M. A consistent co-rotational formulation for non-linear, three-dimensional, beam-elements. Comput Methods Appl Mech Eng August 1990;81(2):131–50.
[9] Ecsedi I, Baksa A. Static analysis of composite beams with weak shear connection. Appl Math Model 2011;35(4):1739–50.
[10] Foraboschi P. Analytical solution of two-layer beam taking into account nonlinear interlayer slip. J Eng Mech 2009;135(10): 1129–46.
[11] Girhammar UA, Gopu VKA. Composite beam-columns with interlayer slip – exact analysis. J Struct Eng 1993;119(4): 1265–82.
[12] Elosta H, Huang Shan, Atilla I. Dynamic response of steel catenary riser using a seabed interaction under random loads. Ocean Eng 2013;69(?):34–43.
[13] Hilber HM, Hughes TJR, Taylor RL. Improved numerical dissipation for time integration algorithms in structural dynamics. Earthq Eng Struct Dyn 1977;5(3):283–92.
[14] Kordkheili SAH, Bahai H, Mirtaheri M. An updated lagrangian finite element formulation for large displacement dynamic analysis of three-dimensional flexible riser structures. Ocean Eng 2011;38(5–6):793–803.
[15] Krawczyk P, Frey F. Large deflections of laminated beams with interlayer slips – part 1: model development. Int J Comput Aided Eng Softw 2007;24(1):17–32.
[16] Lages EN, Paulino GH, Menezes IFM, Silva RR. Nonlinear finite element analysis using an object-oriented philosophy – application to beam elements and to the Cosserat Continuum. Eng Comput 1999;15(1):73–89.
[17] Leon SE, Paulino GH, Pereira A, Menezes IFM, Lages EN. A unified library of nonlinear solution schemes. Appl Mech Rev 2011;64(4). Article 040803.
[18] Malvern LE. Introduction to the mechanics of a continuous medium. Prentice Hall; 1969.
[19] McNamara JF, O'Brien PJ, Gilroy SG. Non-linear analysis of flexible risers using hybrid finite elements. J Offshore Mech Arct Eng 1988;110(3):197–204.
[20] Morison JR, O'Brien MP, Johnson JW, Schaaf SA. The forced exerted by surface waves on piles. Pet Trans 1950;2(5):149–54.
[22] Hosseini Kordkheili SA, Bahai H, Mirtaheri M. An updated Lagrangian finite element formulation for large displacement dynamic analysis of three-dimensional flexible riser structures. Ocean Eng 2011;38(5–6):793–803.
[23] Santillan ST, Virgin LN. Numerical and experimental analysis of the static behavior of highly deformed risers. Ocean Eng 2011;38(13):1397–402.
[24] Schnabl S, Saje M, Turk G, Planinc I. Analytical solution of two-layer beam taking into account interlayer slip and shear deformation. J Struct Eng 2007;133(6):886–94.
[25] Schnabl S, Saje M, Turk G, Planinc I. Locking-free two-layer Timoshenko beam element with interlayer slip. Finite Elem Analysis Des 2007;43(9):705–14.
[26] Simo JC, Vu-Quoc L. A three-dimensional finite strain rod model. Part II: computational aspects. Comput Methods Appl Mech Eng 1986;58(1):79–116.
[27] Wu Y-F, Xu R, Chen W. Free vibrations of the partial-interaction composite members with axial force. J Sound Vib 2007; 299(4–5):1074–93.
[28] Xu R, Wu R, Chen W. Static, dynamic and buckling analysis of partial interaction composite beam theory. Int J Mech Sci 2007;49(10):1139–55.
[29] Yazdchi M, Crisfield MA. Buoyancy forces and the 2D finite element analysis of flexible offshore pipes and risers. Int J Numer Methods Eng 2002;54(1):61–88.
[30] Yazdchi M, Crisfield MA. Non-linear dynamic behavior of flexible marine pipes and risers. Int J Numer Methods Eng 2002; 54(9):1265–308.
[31] Zona A, Ranzi G. Finite element models for nonlinear analysis of steel-concrete composite beams with partial interaction in combined bending and shear. Finite Elem Analysis Des 2011;47(2):98–118.